Catalysis Today 179 (2012) 35–42

Contents lists available at ScienceDirect

Catalysis Today

journal homepage: www.elsevier.com/locate/cattod

Pillared MWW zeolites MCM-36 prepared by swelling MCM-22P in concentrated surfactant solutions

Pavla Chlubná*, Wieslaw J. Roth[1], Arnošt Zukal, Martin Kubů, Jana Pavlatová

J. Heyrovský Institute of Physical Chemistry, Academy of Sciences of the Czech Republic, v.v.i., Dolejškova 3, 182 23 Prague 8, Czech Republic

ARTICLE INFO

Article history:
Received 7 June 2011
Received in revised form 27 June 2011
Accepted 28 June 2011
Available online 29 July 2011

Keywords:
MCM-22 family
MCM-36
MWW structure
X-ray powder diffraction

ABSTRACT

Lamellar zeolite forms like layered MCM-22 precursor, MCM-22P, offer unprecedented opportunities for creating diversity of more open zeolite structures prepared post-synthesis by expanding and modifying the interlamellar space. This is a relatively unexplored area with regard to procedures ensuring easy, least destructive and most efficient expansion of layered zeolites. Herein we explore concentrated surfactant solutions with high pH for their ability to provide swollen MCM-22 that can be converted to the pillared MCM-36. High pH of the swelling solutions was obtained by addition of tetrapropylammonium hydroxide and by partial conversion of the surfactant chloride into hydroxide by ion exchange. The products were evaluated based on their X-ray diffraction characteristics, sorption properties, scanning electron microscopy and IR spectra as indicators of catalytic potential. The swelling/pillaring efficiency was judged based on BET surface area and depended on swelling conditions, especially the apparent basicity. There was an overall decrease in acid site concentration due to incorporation of inert silica pillars. The MCM-36 zeolite with the highest BET showed increased uptake of 2,6-di-tert-butyl-pyridine by 75% compared to the parent MCM-22 suggesting enhanced accessibility of acid sites for bulky probe molecules. We conclude that concentrated surfactant solutions can be effective in swelling MCM-22P even at room temperature but an optimal approach must balance many factors including yield and activity of the final product.

© 2011 Elsevier B.V. All rights reserved.

1. Introduction

Synthetic zeolites demonstrate exceptional benefits as selective heterogeneous catalysts especially in petroleum industry and their synthesis and discovery have been of continuing interest [1–5]. Many structural forms of zeolites are known [6]. They were traditionally obtained by direct synthesis and were not modifiable post-synthesis without degradation as their frameworks were fully connected and extended in three-dimensions (3D). A different class, lamellar 2D solids can be manipulated into different architectures [7,8], especially with expanded interlayer space, based on various packing of constituent layers. Recently the new way of preparation of these lamellar materials was discovered, by post-synthetic treatments of 3D zeolite [9]. However, these 2 D materials are not as active as zeolites, which reduce their application potential. The discovery of layered zeolite precursor MCM-22 [8,10] provided a material combining the desired characteristics from both classes. It also initiated expansion to similar precursors of other zeolite types [11].

As the framework structure MCM-22 has two independent 10-ring pore systems: one sinusoidal intra-layer and one produced by the fusion of the adjacent layers [12]. Additional feature of the layers are 12-ring cavities on the surface [13], which generate approximately 1.8 nm × 0.7 nm supercages inside the crystal. Their presence and accessibility on the external surface of MCM-22 has been postulated as playing a significant role in certain catalytic processes [14–16].

This discovery of a layered form of the catalytically active zeolite MCM-22 was exploited for synthesis of pillared zeolite MCM-36 [17] combining unprecedented mesoporous structure and high zeolite activity. While the developed synthetic procedure was based on known methodology for lamellar solids [18] the critical swelling step proved very demanding and required innovative solution [17]. The conditions ensuring successful swelling proved quite severe, including high concentration of cationic surfactant (hexadecyltrimethylammonium, also called cetyltrimethylammonium, CTMA) and high pH, which could affect quality and integrity of the layers [19]. This has been discussed in a series of publications presenting various aspects of this problem [19–21]. These initial swelling procedures were carried out at elevated temperatures and

* Corresponding author. Tel.: +420 266 053 625.
E-mail addresses: pavla.chlubna@jh-inst.cas.cz (P. Chlubná), wies.roth@gmail.com (W.J. Roth).
[1] Permanent address: 123 Boundbrook Ct., Sewell, NJ 08080, USA.

0920-5861/$ – see front matter © 2011 Elsevier B.V. All rights reserved.
doi:10.1016/j.cattod.2011.06.035

recently studies have been published about its implementation at ambient conditions [22,23].

Steady expansion of the layered zeolite area in the direction of both different frameworks and layered architectures [24] justifies a systematic inquiry into the swelling and pillaring processes, which to date have been carried out under relatively limited conditions, in particular relying on swelling reagent composition used initially and described in the patent [25]. We explored alternative swelling media, such as less dilute surfactant solutions, which can be considered somewhat simpler than those used to date. We evaluated the swelling effectiveness and usefulness based on the porosity properties of the final pillared derivatives. The obtained results are also discussed in terms of their significance for future work and possible wider practical implementation.

2. Experimental

The reagents used, i.e. 25% solution of hexadecyltrimethylammonium chloride (CTMA-Cl), tetrapropylammonium hydroxide (TPA-OH) as 20 and 40% solutions, tetraethylorhosilicate (TEOS) were purchased from Sigma–Aldrich. Hexadecyltrimethylammonium hydroxide solution (CTMA-OH) was obtained by ion exchange of 25% solution of CTMA-Cl with anion exchange resin – 80 ml of resin AG 1-X8 (Bio-Rad) in water drained and mixed with about 100 g of the solution. The slurry was mixed overnight and filtered. A small amount of water 10–20 ml was added during washing.

2.1. Preparation of MCM-22P

MCM-22 was prepared using Ludox LS-30, solid sodium aluminate (50–55% Al_2O_3 and 40–45% Na_2O, Riedel-de-Haen), sodium hydroxide and hexamethyleneimine (HMI) with the following reactant ratios: Si/Al = 18/1, OH−/Si = 0.18, HMI/Si = 0.55 and H_2O/Si = 53. The synthesis mixture with total weight 333 g was loaded into a Teflon-lined Parr reactor (0.5 l) and placed horizontally in an oven on rollers (40 rpm). The hydrothermal synthesis was carried out at 150 °C for 5 days and the product was isolated by standard methods – centrifugation, washing with water, drying at 110 °C. The yield was approximately 16.8 g. The product is designated MCM-22P.

2.2. Swelling of MCM-22P

For exploration of the swelling process different reaction conditions were investigated but with the same initial MCM-22P zeolite.

Swelling with CTMA-OH (**MCM-22-sw1**): 1 g of MCM-22P was stirred overnight at room temperature with 20 ml of the above CTMA-OH solution. The solid was isolated by centrifugation with 2 washings with water (20 ml added, centrifuged, decanted) and dried in air for overnight.

Swelling with CTMA-Cl and TPA-OH at RT (**MCM-22-sw2**): Swelling solution comprising 3 g of 20% TPA-OH and 27 g of 25% hexadecyltrimethylammonium chloride (CTMA-Cl) was mixed with1 g of MCM-22P and stirred overnight. It was isolated and washed like above but dried at 60 °C for overnight.

Swelling with CTMA-Cl and TPA-OH at 95 °C (**MCM-22-sw3**): The above treatment (MCM-22-sw2) was carried out by heating at 95 °C under reflux for overnight.

2.3. Pillaring

Pillaring was carried out with about 0.5 g of dried swollen zeolites from above in about 15 g of TEOS. The mixture was stirred and heated under reflux at 85–95 °C for overnight. The solid was isolated by centrifugation and after decantation of the supernatant TEOS the tube was kept upside down for 6–24 h to drain and evaporate residual TEOS. 20 ml of water was added to the tube and stirred overnight, then centrifuged again and the solid dried at 60 °C. Final calcination was carried out at 540 °C for 3–6 h. The materials were denoted according to the used swollen material **MCM-36-1**, **MCM-36-2** and **MCM-36-3**.

2.4. Characterization

The structure and crystallinity of all zeolites studied was determined by X-ray powder diffraction using a Bruker AXS D8 Advance diffractometer.

Adsorption isotherms of nitrogen at −196 °C were determined using an ASAP 2020 (Micromeritics) static volumetric apparatus. In order to attain sufficient accuracy in the accumulation of the adsorption data, the ASAP 2020 was equipped with pressure transducers covering the 133 Pa, 1.33 kPa and 133 kPa ranges. Before adsorption experiments the zeolite was outgassed under turbomolecular pump vacuum. Starting at ambient temperature the zeolite was outgassed at 110 °C until the residual pressure of 0.5 Pa was obtained. After further heating at 110 °C for 1 h the temperature was increased until the temperature 250 °C of was achieved. This temperature was maintained for 8 h.

The concentration of Lewis (L) and Brønsted (B) acid sites was determined after adsorption of d_3-acetonitrile (ACN) by FTIR spectroscopy on Nicolet Protégé 460 Magna with a transmission DTGS and MTC/A detector. Zeolites were pressed into self-supporting wafers with a density of 8.0–12.0 mg/cm^2 and activated in situ at 450 °C overnight. Before adsorption d_3-acetonitrile was degassed by freezing and thawing cycles. d_3-acetonitrile was adsorbed at ambient temperature for 30 min at partial pressure 900 Pa, followed by desorption for 20 min. All spectra were recorded with resolution of 4 cm^{-1} by collecting 128 scans for a single spectrum at room temperature. The experimental data were recalculated to a normalized wafer (density of 10 mg/cm^2). The concentration of Lewis and Brønsted acid sites were evaluated from the integral intensities of bands at 2323 cm^{-1} (Lewis acid sites) and at 2294 cm^{-1} (Brønsted acid sites) using extinction coefficients, ε (L) = 3.6 cm/μmol, and ε (B) = 2.05 cm/μmol [26]. The presented IR spectra both for d_3-acetonitrile and 2,6-di-tert-butyl-pyridine (DTBP) are not correlated to standard mass.

A large probe molecule DTBP was used to determine the concentration of acid sites located on the external surface of zeolites [27]. The adsorption of DTBP was performed at 150 °C at equilibrium probe vapour pressure with the zeolite wafer for 15 min. Desorption proceeded at the same temperature for 1 h followed by collection of spectra at room temperature. Extinction coefficients for pyridine [28] were used for the quantitative evaluation of the concentration of Lewis and Brønsted acid sites.

The size and shape of zeolite crystals were examined by scanning electron microscopy (SEM, JEOL, JSM-5500LV). For the measurement, crystals were coated with a thin platinum layer by sputtering in vacuum chamber of a BAL-TEC SCD-050.

3. Results and discussion

3.1. Swelling and physical properties of MCM-36

We investigated new conditions for swelling MCM-22P and continued to produce pillared MCM-36 derivatives, which were characterized by XRD, sorption, SEM and IR spectroscopy. The synthetic approach adopted here relied on an undiluted commercial surfactant solution (25% CTMA-Cl) with the necessary high pH generated by addition of TPA-OH (CTMA-TPA) or ion exchange to generate some CTMA-OH hydroxide. The molar concentration of

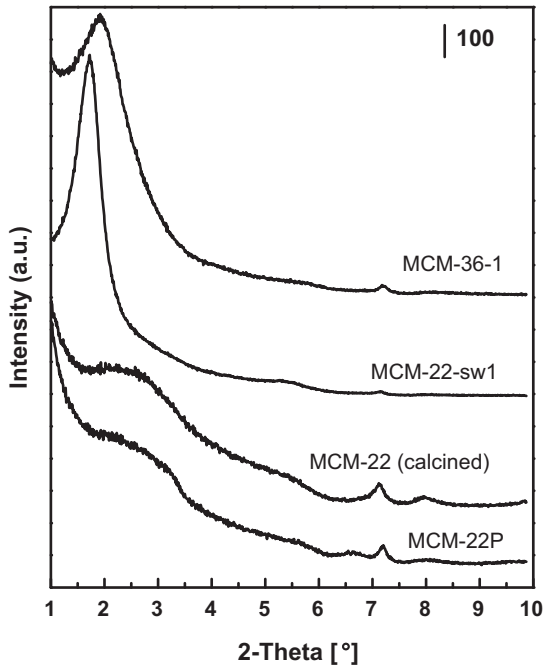

Fig. 1. Low angle X-ray powder diffraction pattern (XRD) of MCM-22P (ammonium exchanged twice) and its calcined product MCM-22 compared to the CTMA-OH swollen (MCM-22-sw1) and pillared (MCM-36-1) materials. The intensities are arbitrarily adjusted for clarity.

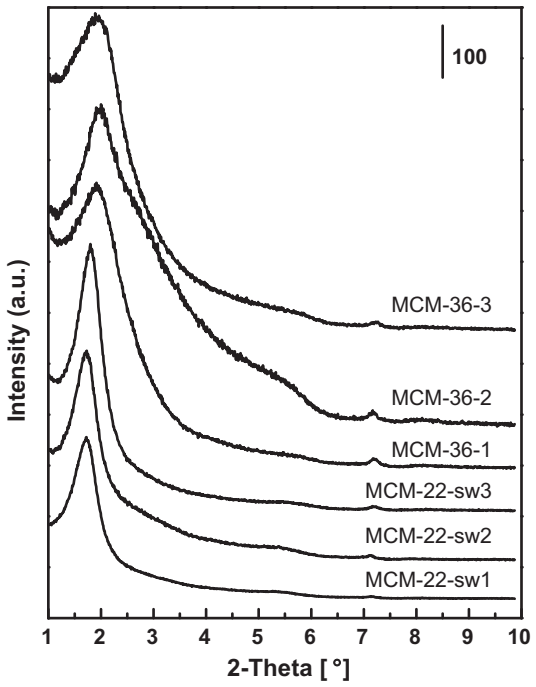

Fig. 2. Low angle XRD pattern of the swollen MCM-22P and final pillared MCM-36 materials. The intensities are arbitrarily adjusted for clarity.

the CTMA-TPA mixture was about 0.7 and 0.1, respectively. MCM-22P zeolite was contacted with the swelling media for overnight, isolated, washed with water, dried, refluxed in TEOS at around 85–95 °C for overnight and hydrolyzed with water. The final product MCM-36 was obtained by calcination at 540 °C.

MCM-22P was prepared based on common procedure with hexamethyleneimine (HMI) as template. Its quality was confirmed by XRD and standard nitrogen sorption determinations carried out with twice ammonium exchanged and calcined zeolite. It showed BET surface area of 535 m^2/g and micropore volume 0.174 cm^3/g, which indicates high quality MWW (MCM-22).

The details of MCM-22P swelling process, characteristics of the products indicating successful swelling and absence of noticeable impurities like MCM-41/M41S have been thoroughly discussed in earlier publications [16,20,22,23].

Briefly, swelling is diagnosed in comparison to the starting MCM-22P by:

(1) appearance of a dominant intense peak below or around 2° $2-\theta$ (Cu Kα radiation throughout) corresponding to ≥4.4 nm d-spacing equal to the lattice constant in the layer stacking direction
(2) unassigned peak at ca. 5.5° $2-\theta$
(3) disappearance of the (0 0 2) reflection at 6.5° $2-\theta$
(4) merging of the (1 0 1) and (1 0 2) reflections at roughly 8 and 10° $2-\theta$ into a broad band preferably without a depression in between.

The 1st dominant reflection at ≤2° $2-\theta$ and the broad band at 8–10° $2-\theta$ are supposed to be retained in the pillared calcined product. There is an inherent difficulty in quantitative evaluation of swollen and pillared zeolites based on XRD patterns ('crystallinity') and therefore the data must be supplemented with adsorption measurements such as nitrogen isotherm determination.

XRD patterns of the zeolites obtained in this work are shown in comparison to the starting MCM-22P in Figs. 1–3 in both low and high angle regions (1–10 and 3–30° $2-\theta$). As remarked above, they allow only qualitative assessment of the swelling efficiency while quantitative appraisal requires sorption data such as BET. The relevant numerical values are listed in Table 1 which also provides interlayer d-spacing values.

All treated zeolites show a low angle line at d-spacing higher than 4.4 nm (≤2° $2-\theta$) suggestive of successful swelling and pillaring. While the (0 0 2) reflection at ~6.5° $2-\theta$ (1.35 nm) is also absent in all cases the zeolite pillared from CTMA-TPA at room temperature treatment, MCM-36-2, shows a distinct depression in the 8–10° $2-\theta$ region diagnostic of small but certain degree

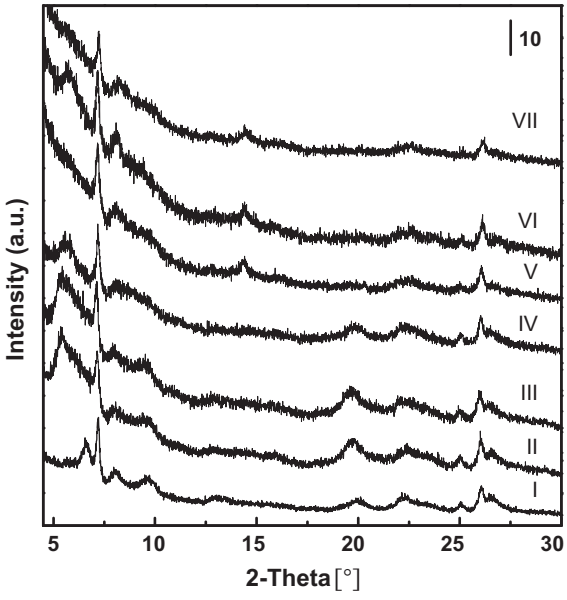

Fig. 3. XRD pattern from 3 to 30° $2-\theta$ for the swollen MCM-22P and final pillared MCM-36 materials. (I) MCM-22P, (II) MCM-22-sw1, (III) MCM-22-sw2, (IV) MCM-22-sw3, (V) MCM-36-1, (VI) MCM-36-2, and (VII) MCM-36-3. The intensities are arbitrarily adjusted for clarity.

Table 1
Interlayer d-spacing and BET surface area values for the MCM-22 derivatives prepared in this work.

	Low angle line XRD		BET (m^2/g)	V_{micro} (cm^3/g)	V_{meso} (cm^3/g)	V_{int} (cm^3/g)	V_{Σ} (cm^3/g)
	$2-\theta$ (°)	d-spacing (nm)					
MCM-22	–	–	536	0.174	–	0.294	0.475
MCM-22-sw1	1.72	5.13	460	0.144	–	0.245	0.396
MCM-22-sw2	1.73	5.10	–	–	–	–	–
MCM-22-sw3	1.80	4.90	–	–	–	–	–
MCM-36-1	1.90	4.65	729	0.056	0.302	0.405	0.740
MCM-36-2	2.00	4.40	578	0.047	0.227	0.209	0.444
MCM-36-3	1.95	4.50	614	0.038	0.263	0.280	0.552

V_{micro} – the volume microporous; V_{meso} – the volume mesoporous; V_{int} – the volume of interparticle space; V_{Σ} – the total pore volume.

incomplete exfoliation. This reflects that this zeolite has only moderately enhanced BET surface area compared to the parent MCM-22 (Table 1). The XRD of MCM-36-3, from the zeolite swollen by CTMA-TPA at higher temperature, seems much improved based on criterion 4 above but the BET increase is quite moderate. Our conclusion, to be tested, is that higher basicity, i.e. more TPA-OH, should be used but not in excess as it may affect integrity of the MCM-22 layers.

Scanning electron images of initial MCM-22, the swollen one and MCM-36 are depicted in Fig. 4. The zeolites differ somewhat with regard to size of individual crystals and their aggregation. The morphology of individual crystals of all zeolites is characterized by plate shape. The crystal size of MCM-22 prepared with initial n_{Si}/n_{Al} molar ratio of 18 is about 1.0 μm × 0.7 μm × 0.1 μm (Fig. 4A) but there are also large crystal aggregates present. In the MCM-36 the size of crystals appears increased to about 2.0 μm × 1.0 μm × 0.1 μm (Fig. 4C). The simplest explanation is that these sizes reflect crystals that were previously hidden in the aggregates that became revealed upon swelling and pillaring treatments. We cannot think of a phenomenon that might cause crystal size enhancement. As expected the swollen zeolite MCM-22-sw1 (Fig. 4B) exhibits a significant tendency to aggregation caused by

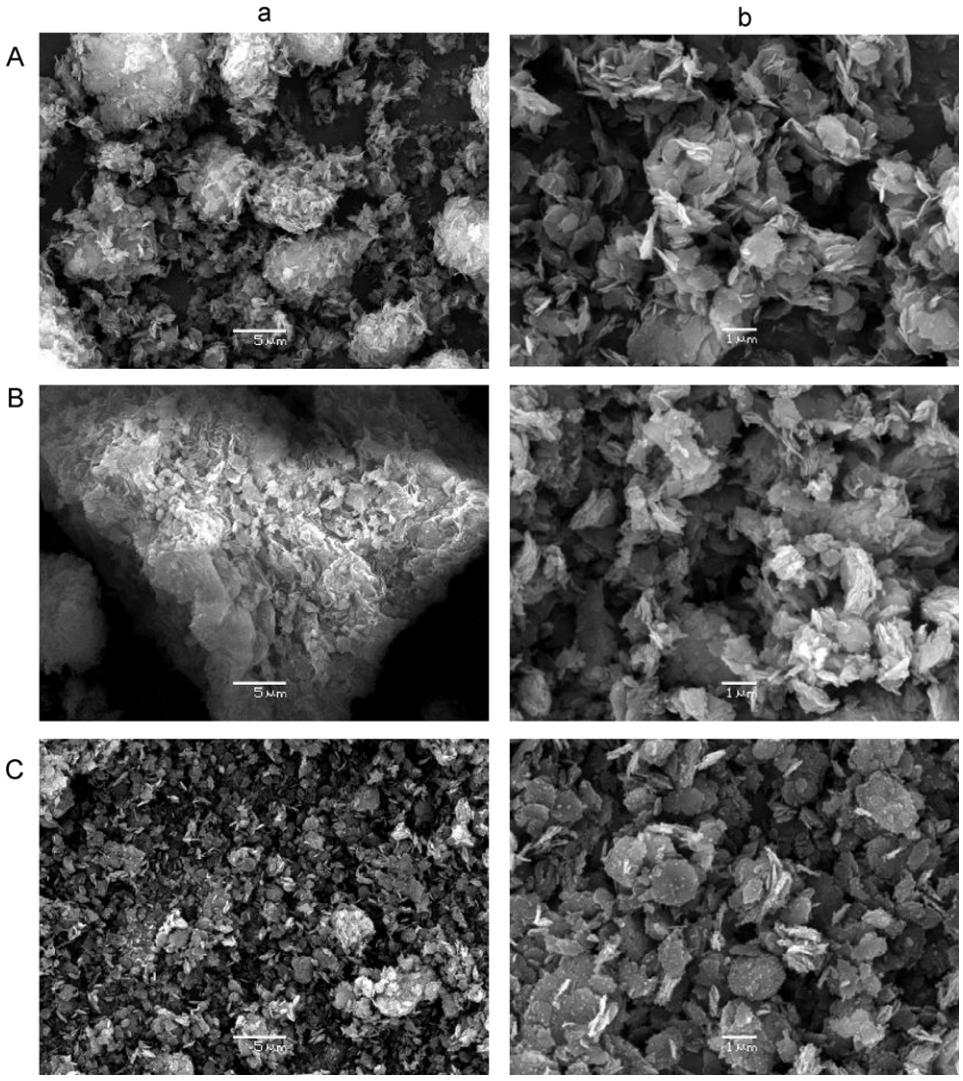

Fig. 4. SEM images of initial MCM-22 (A), MCM-22-sw1 (B) and MCM-36-1 (C) under different magnification: 3000 (a) and 10,000 (b).

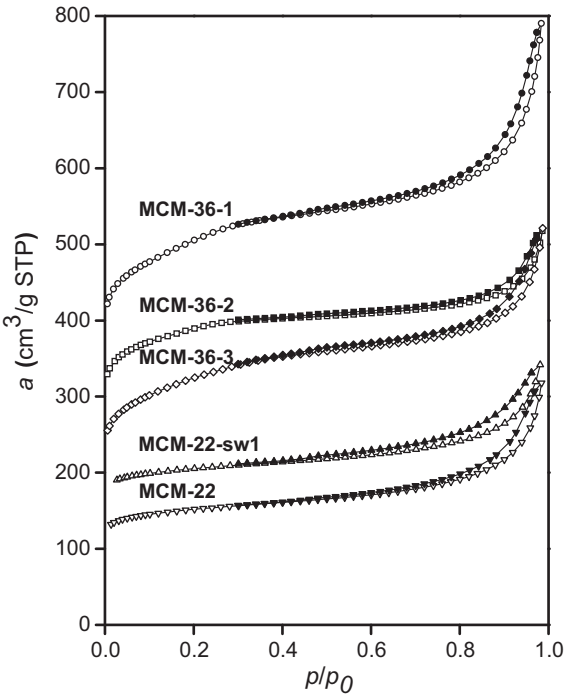

Fig. 5. Nitrogen isotherms at −196 °C. With exception of the zeolite MCM-22 (▽) the isotherms are shifted vertically by 75 cm^3/g STP (△, MCM-22-sw1), 150 cm^3/g STP (◊, MCM-36-3), 225 cm^3/g STP (□, MCM-36-2), and 300 cm^3/g STP (◯, MCM-36-1), respectively. Solid points denote desorption.

the treatment which led to delamination (chemical treatment plus calcination).

3.2. Textural properties

The textural parameters of zeolites under study were evaluated based on nitrogen isotherms presented in Fig. 5. All the isotherms reveal type H3 hysteresis loop, which is observed with non-rigid aggregates of plate-like particles giving rise to slit-shaped mesopores. This conclusion is supported by SEM images shown in Fig. 4. The BET surface area, S_{BET}, was evaluated using adsorption data in a relative pressure range from $p/p_0 = 0.05$ to $p/p_0 = 0.22$. The adsorbed amount at relative pressure $p/p_0 = 0.98$ reflects the total adsorption capacity. Therefore, the total pore volume V_Σ could be calculated by converting the total amount adsorbed into liquid volume. The values of determined surface areas and total pore volumes are summarized in Table 1. To obtain information about the microporous and mesoporous structures, *t*-plot and DFT methods were applied. The application of the *t*-plot method has enabled us to determine the micropore volume V_{micro}. The data reveal that unlike the zeolites MCM-22 and MCM-22-sw1 ($V_{micro} = 0.174$, 0.144 cm^3/g, respectively), the values of micropore volumes of all pillared zeolites MCM-36-1, MCM-36-2, and MCM-36-3 are much lower, between 0.038 and 0.056 cm^3/g. The texture analysis of these pillared zeolites based on the DFT method (using standard Micromeritics software for slit-shaped pores) assessed a presence of smaller mesopores of volume V_{meso} (Table 1) with distribution centered at width of 2.5 nm. The volume V_{int} (Table 1) of larger voids was calculated from the desorption branch of the hysteresis loop using the BJH algorithm. All zeolites possess a wide range of larger free voids which spans sizes from 4 nm to 50 nm without discernible maximum. This void volume represents nitrogen adsorption in the interparticle space.

Table 1 shows the increase in the BET surface area from initial MCM-22 zeolite to pillared zeolites, MCM-36, in accordance with the synthesis procedure. The changes of micropore volume V_{micro} and mesopore volume V_{meso} reflect structural changes caused by the swelling followed by pillaring. The initial micropore structure and volume of zeolite MCM-22 is reduced as it is only preserved in the inter-layer pore system. The rest, i.e. initially between the layers, vanishes due to the efficient expansion and formation of interlamellar space. At the same time, the total pore volume increases from the initial MCM-22 to pillared MCM-36 as a consequence of the changed particle morphology and formation of larger mesopores.

As mentioned above one of the dangers of the aggressive chemical environment during swelling treatment is the possibility of generation of M41S-type materials, which would contribute to apparent enhanced BET surface area and adsorption capacity. Even the collapsing and XRD invisible upon calcination of lamellar MCM-50 retains considerable porosity and BET values [29]. One of the tests addressing this issue is calcination of the swollen product and measurement of sorption. In this case (Table 1) the BET of the swollen and calcined control material, MCM-22-sw1, was below that of the starting MCM-22 proving that no significant mesoporous impurities were generated.

3.3. Acidity characterization by FTIR

The ultimate practical goal of the examined transformation into the pillared derivative is generation of a better catalyst in comparison to the untreated zeolite. In general, this is dependent on a particular catalytic process. In the case like MCM-22, which is a very active and effective catalyst, the presence of inert pillars in MCM-36 puts the latter at a disadvantage by diminishing overall acidity, while the process of swelling and pillaring may degrade the existing centers. Nonetheless, clearly superior performance of MCM-36 even with diminished overall acidity has been documented in olefin/isobutane alkylation [30,31].

In Fig. 6A, C the IR spectra of parent MCM-22 and treated zeolites (MCM-22-sw1, MCM-36) in the region of OH stretching vibration are shown. The sharp absorption band with the highest intensity found at 3745 cm^{-1} is assigned to the terminal silanol groups exposed at the external surface, while the broader band at 3622–24 cm^{-1} is related to acidic bridging Si–(OH)–Al groups. The parent MCM-22 and the swollen MCM-22-sw1 show an indication of a very weak band between 3660 and 3670 cm^{-1}, which is characteristic for OH groups located on extra-framework aluminum centers [32]. This band is usually observed in high-silica zeolites at the lowest region of Si/Al [33]. Some of these aluminum-containing species reveal the Brønsted-type acidity [34]. d_3-acetonitrile adsorption – Fig. 6B, D – led to the complete coverage of bridging hydroxyl groups (3622–24 cm^{-1}) with the corresponding appearance of two absorption bands at 2292–94 and 2323–25 cm^{-1} as a result of the interaction of d_3-acetonitrile with Brønsted and Lewis acid sites, respectively. While the intensity of band assigned to terminal silanols (Fig. 6A, C, MCM-22-sw1, MCM-36) is increasing due to addition of silica into the structure, the intensity of bridging Si–(OH)–Al groups is decreasing with the drop of aluminum concentration (Table 2).

As expected, the pillared zeolites showed a decrease in the concentration of Brønsted acid sites as well as Lewis acid sites by roughly half. Simultaneously there was no real significant change in the proportional ratio of Brønsted and Lewis site concentration due to pillaring. The most pronounced effect can be seen with MCM-22-sw1 (swollen and calcined). The number of Lewis sites increases from 0.18 mmol/g (parent MCM-22) to 0.24 mmol/g (MCM-22-sw1), which is consistent with the fact that it is essentially a recovered MCM-22 processed under conditions conducive to dealumination and degradation (chemical treatment plus calcination with abundant organic inside).

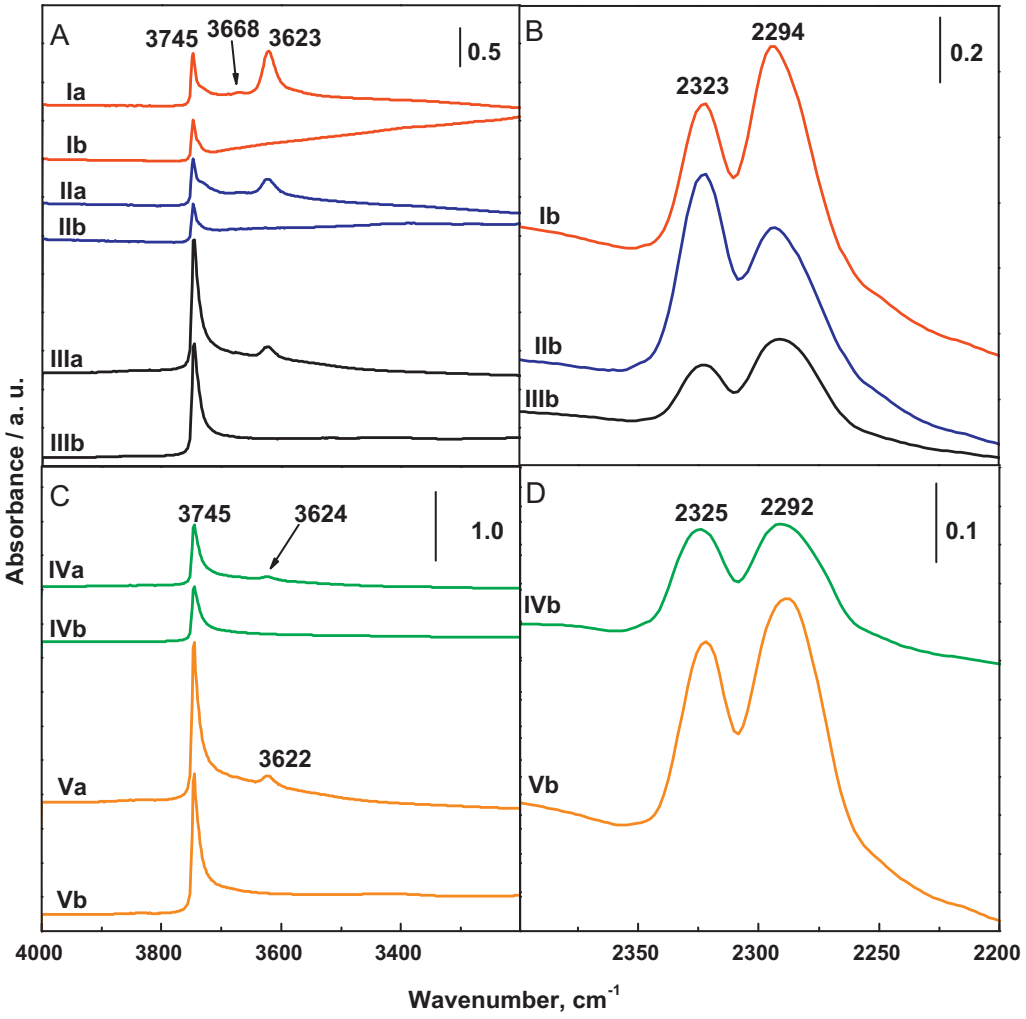

Fig. 6. IR spectra of MCM-22 and derivates, region of hydroxyl vibration (A, C), region of d_3-acetonitrile vibration (B, D), before adsorption (a), after d_3-acetonitrile adsorption (b). (I) MCM-22, (II) MCM-22-sw1, (III) MCM-36-1, (IV) MCM-36-2, and (V) MCM-36-3.

In contrast to majority of other zeolites, MCM-22 contains hydroxyl groups located at the external surface of the zeolite crystals, namely inside the 12-ring pockets. To study accessibility of these groups, 2,6-di-tert-butyl-pyridine adsorption was performed. In comparison with the d_3-acetonitrile adsorption, no differences were observed in the shape and intensity of bands in the region of hydroxyl vibrations before and after the adsorption of DTBP (Fig. 7A, C). The adsorption band at 1535 cm^{-1} is typical for DTBP interacting with Brønsted acid sites. The absence of a band at 1545 cm^{-1} confirms no dealkylation of the probe molecules used (Fig. 7B, D). All performed treatments led to the decrease in the concentration of aluminum (from 1.15 to 0.99, 0.68, 0.56, 0.50 mmol/g) and together with the introduction of silica (in form of TEOS) in the structure caused the increase of Si/Al ratio.

When compared the parent MCM-22, swollen MCM-22-sw1 and pillared zeolites MCM-36, the highest concentration of Brønsted sites located on the external surface was observed on pillared MCM-36-1 (c_B = 0.07 mmol/g). The increased uptake of DTBP by 75% related to the parent material (c_B = 0.04 mmol/g) is in a good agreement with enhanced accessibility of acid sites for bulky probe molecules and corresponds well with the increase in BET area from 536 to 729 m^2/g for parent MCM-22 and pillared MCM-36-1, respectively (Tables 1 and 2). Presumably this can be the advantage in some relevant catalytic process. On the other hand, the swollen MCM-22-sw1 possessed a significant decrease in the external acidity from 0.04 (MCM-22) to 0.01 mmol/g as it was expected due to the degradation of the structure after calcination.

Table 2
Acid center concentrations in MCM-22 and MCM-36.

	c_L (mmol/g)	c_B (mmol/g)	c_{Al} (mmol/g)	Si/Al (IR)	%$_L$	%$_B$	c_B (I) (mmol/g)
MCM-22	0.18	0.78	1.15	13.5	19	81	0.04
MCM-22-sw1	0.24	0.50	0.99	15.8	32	68	0.01
MCM-36-1	0.09	0.38	0.56	28.7	19	81	0.07
MCM-36-2	0.10	0.29	0.50	32.5	26	74	0.02
MCM-36-3	0.12	0.44	0.68	23.6	21	79	0.02

c_L – concentration of Lewis acid sites; c_B – concentration of Brønsted acid sites; c_{Al} – concentration of aluminum; c_B (I) – concentration of Brønsted acid sites located on the external surface.

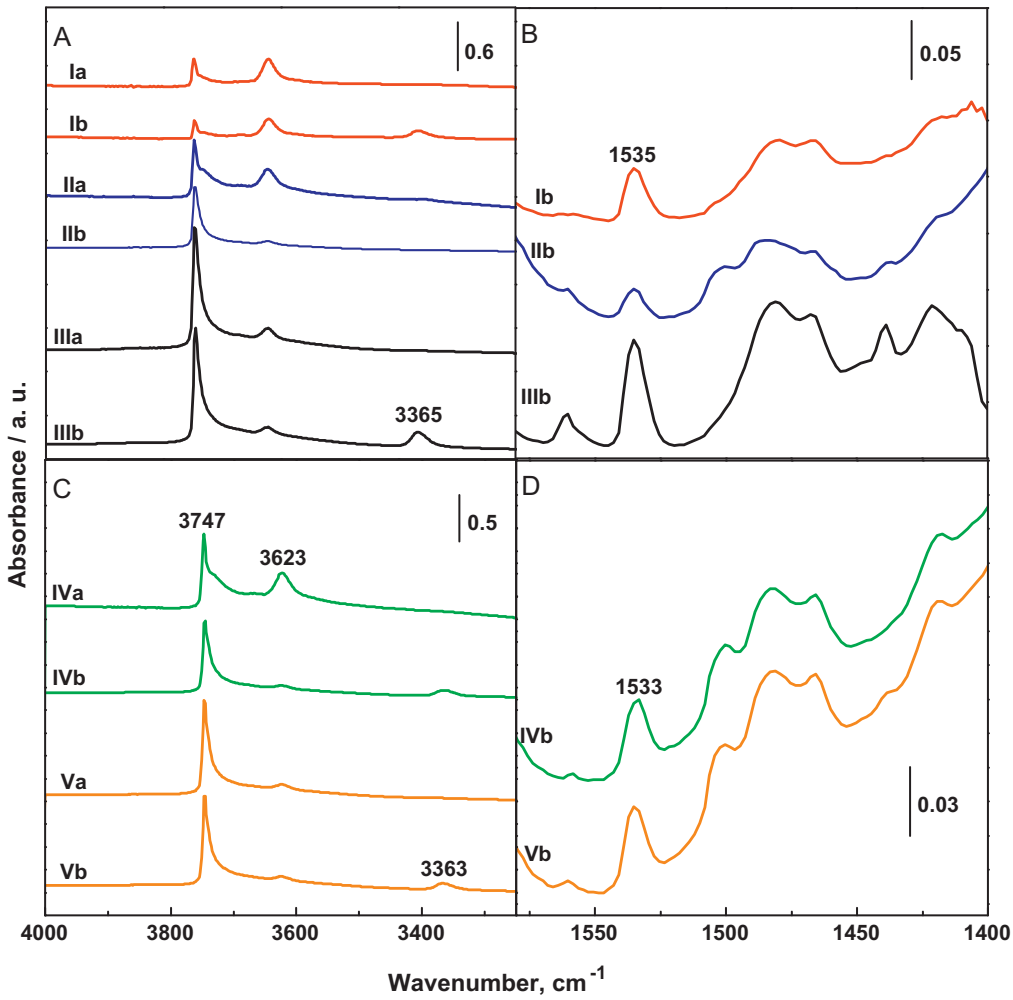

Fig. 7. IR spectra of MCM-22 and derivates, swollen and pillared zeolites, region of hydroxyl vibration (A, C), region of 2,6-di-tert-butyl-pyridine vibration (B, D), before adsorption (a), after adsorption (b). (I) MCM-22, (II) MCM-22-sw1, (III) MCM-36-1, (IV) MCM-36-2, and (V) MCM-36-3.

4. Conclusions

Concentrated surfactant solutions with pH adjusted by addition of TPA-OH or anion exchange were used to swell MCM-22P at room as well as elevated temperature. The efficiency could be judged by XRD (qualitative) and N_2 sorption (quantitative). FTIR proved to be useful in appraising catalytic activity potential of the complex product. It also revealed enhanced access of bulky probe molecule in the case of MCM-36-1 with the highest BET surface area.

The result of this study is the expanded range of swelling conditions, especially with regard to the swelling mixture compositions and the effect of elevated temperature. Still more thorough investigation may be required for a catalytic process where MCM-36 will be a serious candidate for practical implementation. In that case additional factors will have to be evaluated like optimized ratio of swelling medium to precursor being swollen, yield as reflection of possible solid dissolution or degradation, and possible re-use of the swelling solution.

Acknowledgements

The authors thank the Academy of Sciences of the Czech Republic (KAN100400701), the Grant agency of the Czech Republic (104/09/0561) for the support and RNDr. Libor Brabec, CSc. for SEM images.

References

[1] J. Čejka, H. van Bekkum, A. Corma, F. Schuth (Eds.), Introduction to Zeolite Science and Practice, 3rd revised edition, Stud. Surf. Sci. Catal., vol. 168, Elsevier, 2007.
[2] R. Xu, W. Pang, J. Yu, Q. Huo, J. Chen, Chemistry of Zeolites and Related Porous Materials , Wiley, Singapore, 2007.
[3] C.S. Cundy, P.A. Cox, Chem. Rev. 103 (2003) 663.
[4] J. Jiang, J. Yu, A. Corma, Angew. Chem. Int. Ed. 49 (2010) 3120.
[5] N. Žilková, M. Bejblová, B. Gil, S.I. Zones, A.W. Burton, C.-Z. Chen, Z. Musilová-Pavlačková, G. Košová, J. Čejka, J. Catal. 266 (2009) 79.
[6] C. Baerlocher, W.M. Maier, D.H. Olson, Atlas of Zeolite Framework Types , 6th ed., Elsevier, Amsterdam, 2007.
[7] S.M. Auerbach, K.A. Carrado, P.K. Datta, Handbook of Layered Materials , Marcel Dekker, New York, 2004.
[8] K. Ohtsuka, Chem. Mater. 9 (1997) 2039.
[9] W.J. Roth, O.V. Shvets, M. Shamzhy, P. Chlubná, M. Kubů, P. Nachtigall, J. Čejka, J. Am. Chem. Soc. 133 (2011) 6130.
[10] L. Lawton, A.S. Fung, G.J. Kennedy, L.B. Alemany, C.D. Chang, G.H. Hatzikos, D.N. Lissy, M.K. Rubin, H.-K.C. Timken, J. Phys. Chem. 100 (1996) 3788.
[11] W.J. Roth, in: J. Čejka, H. van Bekkum, A. Corma, F. Schuth (Eds.), Introduction to Zeolite Science and Practice, 3rd edition, Stud. Surf. Sci. Catal., vol. 168, Elsevier, Amsterdam, 2007, pp. 221–239.
[12] M.E. Leonowicz, J.A. Lawton, S.L. Lawton, M.K. Rubin, Science 264 (1994) 1910.
[13] S.L. Lawton, M.E. Leonowicz, R.D. Partridge, P. Chu, M.K. Rubin, Micropor. Mesopor. Mater. 23 (1998) 109.
[14] J.C. Cheng, T.F. Degnan, J.S. Beck, Y.Y. Huang, M. Kalyanaraman, J.A. Kowalski, C.A. Loehr, D.N. Mazzone, Stud. Surf. Sci. Catal. 121 (1999) 53.
[15] J. Čejka, A. Krejčí, N. Žílková, J. Kotrla, S. Ernst, A. Weber, Micropor. Mesopor. Mater. 20 (2002) 397.
[16] A. Corma, V. Fornés, J. Catal. 135 (2001) 73.
[17] W.J. Roth, J. Čejka, Catal. Sci. Technol. 1 (2011) 43.

[18] W.J. Roth, C.T. Kresge, J.C. Vartuli, M.E. Leonowicz, A.S. Fung, S.B. McCullen, in: H.K. Beyer, H.G. Karge, I. Kiricsi, B. Nagy (Eds.), Catalysis by Microporous Materials, Stud. Surf. Sci. Catal., vol. 94, Elsevier, New York, 1995, pp. 301–308.
[19] W.J. Roth, J.C. Vartuli, C.T. Kresge, in: A. Sayari, M. Jaroniec, T.J. Pinnavaia (Eds.), Nanoporous Materials II, Stud. Surf. Sci. Catal., vol. 129, Elsevier, New York, 2000, pp. 501–508.
[20] W.J. Roth, Pol. J. Chem. 80 (2006) 703.
[21] W.J. Roth, J.C. Vartuli, in: A. Sayari, M. Jaroniec (Eds.), Nanoporous Materials III, Stud. Surf. Sci. Catal., vol. 141, Elsevier, New York, 2002, pp. 273–279.
[22] S. Maheshwari, E. Jordan, S. Kumar, F.S. Bates, R.L. Penn, D.F. Shantz, M. Tsapatsis, J. Am. Chem. Soc. 130 (2008) 1507.
[23] S. Maheshwari, C. Martinez, M.T. Portilla, F.J. Llopis, A. Corma, M. Tsapatsis, J. Catal. 272 (2010) 298.
[24] W.J. Roth, D.L. Dorset, Micropor. Mesopor. Mater. 142 (2011) 32.
[25] C.T. Kresge, W.J. Roth, K.G. Simmons, J.C. Vartuli, U.S. Patent 5,229,341 (1993).
[26] B. Gil, S.I. Zones, S.-J. Hwang, M. Bejblová, J. Čejka, J. Phys. Chem. C 112 (2008) 2997.
[27] A. Corma, V. Fornés, L. Forni, F. Márquez, J.M. Triguero, D. Moscotti, J. Catal. 179 (1998) 451.
[28] C.A. Emeis, J. Catal. 141 (1993) 347.
[29] M. Kruk, M. Jaroniec, M.L. Pena, F. Rey, Chem. Mater. 14 (2002) 4434.
[30] E.J.A. Schweitzer, P.F. van den Oosterkamp, Micropor. Mesopor. Mater. 20 (1998) 397.
[31] Y.J. He, G.S. Nivarthy, F. Eder, K. Seshan, J.A. Lercher, Micropor. Mesopor. Mater. 25 (1998) 207.
[32] J.A. Lercher, C. Grundling, G. Eder-Mirth, Catal. Today 27 (1996) 353.
[33] J. Datka, B. Sulikowski, B. Gil, J. Phys. Chem. 100 (1996) 11242.
[34] B. Gil, B. Marszałek, A. Micek-Ilnicka, Z. Olejniczak, Top. Catal. 53 (2010) 1340.